ANNALS OF THE ORADEA UNIVERSITY
Fascicle of Management and Technological Engineering
ISSUE #1, MAY 2013, http://www.imtuoradea.ro/auo.fmte/

CIRCULAR-AXIS FLEXURE HINGES

Nicolae LOBONTIU[1], Matthew CULLIN[2], Jeffrey HOFFMAN[3], Muhammad ALI[4]
[1]University of Alaska Anchorage, USA, nlobontiu@uaa.alaska.edu
[2]University of Alaska Anchorage, USA, mcullin@uaa.alaska.edu
[3]University of Alaska Anchorage, USA, jahoffman@uaa.alaska.edu
[4]Ohio University, Athens, USA, mali5@uaa.alaska.edu

***Abstract*—**The paper introduces the analytical planar compliance model of circular-axis symmetric notch flexure hinges that can be used as flexible connectors in compliant mechanisms. The circular-axis flexure design adds an extra parameter, the median circle radius, to the regular straight-axis flexure design domain. Six general compliances are derived with respect to an end reference frame in terms of only three compliances of half the flexure hinge. Two new circular-axis configurations are studied, namely: the right circular flexure and the right circularly corner-filleted flexure hinge. The analytical compliance model predictions of the two designs are confirmed by finite element simulation and experimental tests.

***Keywords*—**flexure, hinge, compliance, circular

I. INTRODUCTION

FLEXURE hinges are elastic portions that are built monolithically with rigid links to form compliant (or flexible) mechanisms. The flexure hinges mainly deform in bending and are the counterparts of typical rotation pairs in regular linkages. They have several advantages over rotation joints including compactness, no friction losses, lack of lubrication, and minimal assembly. Flexure-based compliant mechanisms are used in a wide variety of macro- and micro/nano-scale applications such as sensors, actuators, robotics, precision positioning devices, grippers, and orthotics [1] – [9], but also optomechanics – [10] and linear/rotary monolithic bearings – [11], [12].

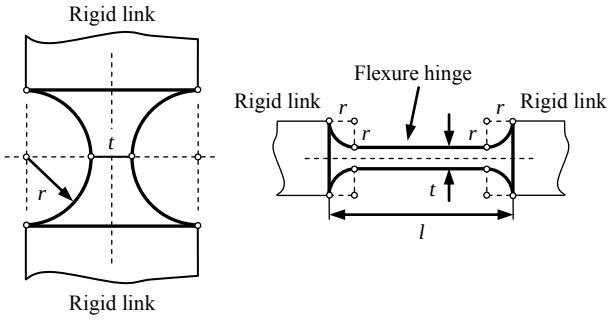

Fig. 1. Two common straight-axis flexure hinges: (a) Right circular; (b) Right circularly corner-filleted

To change the motion characteristics of a flexure hinge, shape variation is most often utilized, particularly in a predefined design envelope. Usually the flexures' shapes are defined by curves that enable the analytical formulation of compliances – the main qualifiers of the quasi-static response of flexures. The overwhelming majority of flexure designs have straight longitudinal axis and Fig. 1 illustrates two of the most common configurations: the right circular flexure hinge – Fig. 1(a) – and the right circularly corner-filleted flexure hinge of Fig. 1(b).

More recently, circular-axis flexure hinges have been introduced – [13], [14] – such as the ones illustrated in Fig. 2, which are the counterparts of the designs shown in Fig. 1.

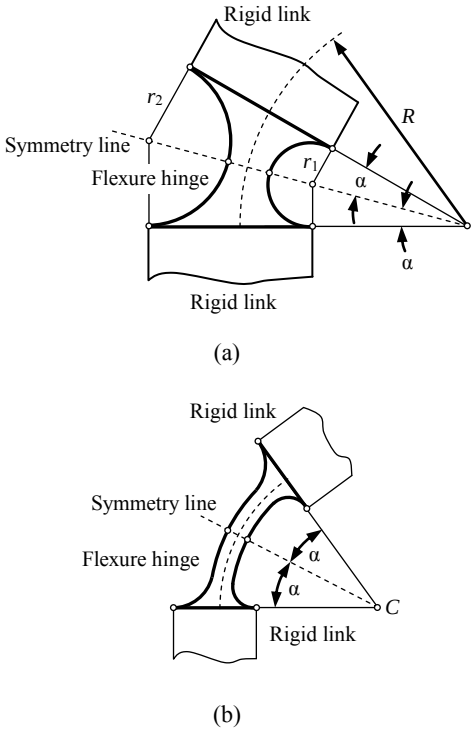

Fig. 2. Circular-axis flexure hinges: (a) Right circular; (b) Right circularly corner-filleted (radius of median circle is *R*)

The paper derives the six planar analytic compliances defining the quasi-static response of a generic symmetric circular-axis flexure hinge by expressing them in terms of only three compliances characterizing half the symmetric

flexure. The particular compliances of the flexure configurations depicted in Fig. 2 are subsequently obtained. The analytic predictions are then compared to finite element analysis (FEA) and experimental results.

II. General Analytical Compliances

Consider a generic circular-axis flexure hinge, which is symmetric with respect to a radial direction – see Fig. 3(a) – and whose half structure is pictured in Fig. 3(b). The in-plane thickness t varies as a function of the variable position β whereas the out-of-plane dimension, w, is constant.

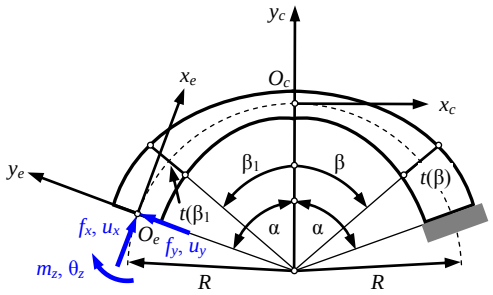

(a)

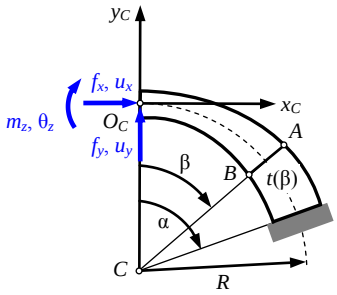

(b)

Fig. 3. (a) Symmetric circular-axis flexure hinge; (b) Half flexure hinge – both shown with end load and deformations

The loads and the corresponding small deformations at the flexure's free end in Fig. 3(a) are connected by means of the following compliance matrix:

$$\begin{bmatrix} \theta_z \\ u_x \\ u_y \end{bmatrix} = \begin{bmatrix} C_{\theta_z-m_z} & C_{\theta_z-f_x} & C_{\theta_z-f_y} \\ C_{\theta_z-f_x} & C_{u_x-f_x} & C_{u_x-f_y} \\ C_{\theta_z-f_y} & C_{u_x-f_y} & C_{u_y-f_y} \end{bmatrix} \begin{bmatrix} m_z \\ f_x \\ f_y \end{bmatrix} \quad (1)$$

The subscript pair of any compliance in Eq. (1) indicates the deformation at the flexure's end (θ_z, u_x or u_y) and the particular load (m_z, f_x or f_y) directly related to a specific deformation.

As demonstrated in [13] and [14], the compliances of the full flexure of Fig. 3(a) are calculated in terms of only three compliances of the half flexure hinge of Fig. 3(b) – the latter ones being denoted by the superscript h, namely:

$$\begin{cases} C_{\theta_z-m_z} = 2C^h_{\theta_z-m_z}; \\ C_{\theta_z-f_x} = 2R(1-\cos\alpha)C^h_{\theta_z-m_z} + 2\cos\alpha \cdot C^h_{\theta_z-f_x}; \\ C_{\theta_z-f_y} = 2R\sin\alpha \cdot C^h_{\theta_z-m_z} - 2\sin\alpha \cdot C^h_{\theta_z-f_x}; \\ C_{u_x-f_x} = 2R^2(1-\cos\alpha)^2 \cdot C^h_{\theta_z-m_z} + 4R[\cos\alpha - \cos(2\alpha)] \cdot C^h_{\theta_z-f_x} \\ +2\cos(2\alpha) \cdot C^h_{u_x-f_x}; \\ C_{u_x-f_y} = 2R^2[\sin\alpha - \sin(2\alpha)/2] \cdot C^h_{\theta_z-m_z} + 2R[2\sin(2\alpha) - \sin\alpha] \cdot C^h_{\theta_z-f_x} \\ -2\sin(2\alpha) \cdot C^h_{u_x-f_x}; \\ C_{u_y-f_y} = 2R^2\sin^2\alpha \cdot C^h_{\theta_z-m_z} + 4R\cos(2\alpha) \cdot C^h_{\theta_z-f_x} - 2\cos(2\alpha) \cdot C^h_{u_x-f_x} \end{cases} \quad (2$$

)

with the half flexure compliances being determined as:

$$\begin{cases} C^h_{\theta_z-m_z} = \dfrac{12R}{Ew} \cdot \displaystyle\int_0^\alpha \dfrac{d\beta}{t(\beta)^3}; \\ C^h_{\theta_z-f_x} = \dfrac{12R^2}{Ew} \cdot \displaystyle\int_0^\alpha \dfrac{(1-\cos\beta) \cdot d\beta}{t(\beta)^3}; \\ C^h_{u_x-f_x} = \dfrac{12R^3}{Ew} \cdot \displaystyle\int_0^\alpha \dfrac{(1-\cos\beta)^2 \, d\beta}{t(\beta)^3}; \end{cases} \quad (3)$$

III. Right Circular Flexure Hinge

The generic Eqs. (2) and (3) are applied to the right circular flexure hinge of Fig. 2(a), which was studied in more detail in [13]. The geometry of half the symmetric flexure is pictured in Fig. 4.

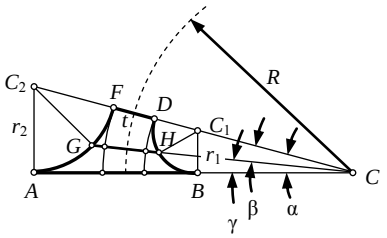

Fig. 4. Half of the circular-axis symmetric right circular flexure hinge with defining geometry

The two fillet radii of Fig. 4 are calculated as:

$$r_1 = \frac{(R - t/2)\sin\alpha}{1+\sin\alpha}; r_2 = \frac{(R + t/2)\sin\alpha}{1-\sin\alpha} \quad (4)$$

whereas the variable thickness is determined as:

$$t(\beta) = \frac{r_2 \sin\delta - r_1 \sin[\varepsilon + \beta]}{\sin\beta} \tag{5}$$

with the angles δ and ε being:

$$\begin{cases} \delta = \sin^{-1}\left(\dfrac{R + t/2 + r_2}{r_2} \cdot \sin\beta\right) - \beta; \\ \varepsilon = \sin^{-1}\left(\dfrac{R - t/2 - r_1}{r_1} \cdot \sin\beta\right) \end{cases} \tag{6}$$

The following numerical parameters have been used to obtain the numerical compliances of the right circular flexure hinge of Fig. 2(a): R = 0.08175 m, $\alpha = 8^o$, t = 0.0015113 m, w = 0.00635 m, r_1 = 0.0098951 m, r_2 = 0.013339 m. The material is aluminum with $E = 71 \times 10^9$ N/m^2 and $\mu = 0.33$.

The finite element package ANSYS has been used with a model illustrated in Fig. 5. The mesh was generated by means of planar shell-type elements with three degrees of freedom per node. Three separate loads (forces about the x and y directions, as well as a moment about the z direction) have been applied at the test point in Fig. 5, followed by reading the resulting displacements at the same point. This process enabled calculation of the FEA compliances as:

$$\begin{cases} C_{u_x - f_x} = \dfrac{u_x}{f_x}; C_{u_y - f_x} = \dfrac{u_y}{f_x} = \dfrac{u_x}{f_y} = C_{u_x - f_y}; \\ C_{\theta_z - f_x} = \dfrac{\theta_z}{f_x} = \dfrac{u_x}{m_z} = C_{u_x - m_z}; C_{u_y - f_y} = \dfrac{u_y}{f_y}; \\ C_{\theta_z - f_y} = \dfrac{\theta_z}{f_y} = \dfrac{u_y}{m_z} = C_{u_y - m_z}; C_{\theta_z - m_z} = \dfrac{\theta_z}{m_z} \end{cases} \tag{7}$$

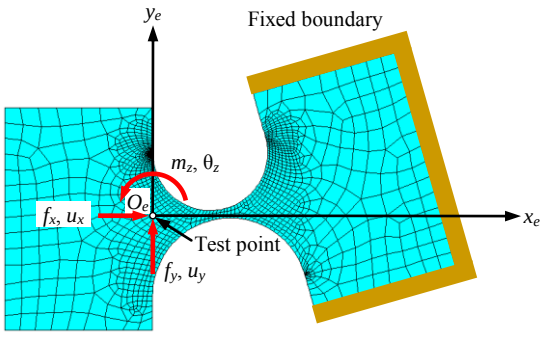

Fig. 5. Finite element model of the right circular flexure hinge prototype

The experimental setup pictured in Fig. 6 was utilized to verify the analytical model accuracy.

Fig. 6. Experimental setup for measuring the planar compliances

Three displacement sensors were employed to measure the vertical and horizontal displacements produced by various loads. Simple geometric relationships were applied thereafter to determine the equivalent displacements at the test point (shown in Fig. 5). The experimental compliances (indicated by superscript e below) were subsequently calculated based on the equation:

$$\begin{bmatrix} C^{(e)}_{\theta_z - m_z} & C^{(e)}_{\theta_z - f_x} & C^{(e)}_{\theta_z - f_y} \\ C^{(e)}_{u_x - m_z} & C^{(e)}_{u_x - f_x} & C^{(e)}_{u_x - f_y} \\ C^{(e)}_{u_y - m_z} & C^{(e)}_{u_y - f_x} & C^{(e)}_{u_y - f_y} \end{bmatrix} = \begin{bmatrix} \theta_{z,(a)} & \theta_{z,(b)} & \theta_{z,(c)} \\ u_{x,(a)} & u_{x,(b)} & u_{x,(c)} \\ u_{y,(a)} & u_{y,(b)} & u_{y,(c)} \end{bmatrix} \begin{bmatrix} m_{z,(a)} & m_{z,(b)} & m_{z,(c)} \\ f_{x,(a)} & f_{x,(b)} & f_{x,(c)} \\ f_{y,(a)} & f_{y,(b)} & f_{y,(c)} \end{bmatrix}^{-1} \tag{8}$$

where a, b, and c denote the three different load cases – see [13] for more details.

The analytical model predictions matched well the FEA and experimental results, the maximum relative error being 9% and corresponding to the $C_{ux\text{-}fx}$ force-deflection translatory compliance.

IV. Right Circularly Corner-Filleted Flexure Hinge

The same generic Eqs. (2) and (3) were used to obtain the compliances of a right circularly corner-filleted flexure hinge prototype – [14] – of the shape illustrated in Fig. 2(b) and whose half component is sketched in Fig. 7.

The compliances defining the half flexure hinge of Fig. 7 are calculated as detailed in [14]:

$$\begin{cases} C^h_{\theta_z-m_z} = C^1_{\theta_z-m_z} + C^2_{\theta_z-m_z}; \\ C^h_{\theta_z-f_x} = C^1_{\theta_z-f_x} + R\left(1-\cos\alpha_1\right)C^2_{\theta_z-m_z} \\ +\cos\alpha_1 \cdot C^2_{\theta_z-f_x} + \sin\alpha_1 \cdot C^2_{\theta_z-f_y}; \\ C^h_{u_x-f_x} = C^1_{u_x-f_x} + R^2\left(1-2\cos\alpha_1+\cos^2\alpha_1\right)C^2_{\theta_z-m_z} \\ +2R\left[\cos\alpha_1-\cos\left(2\alpha_1\right)\right]C^2_{\theta_z-f_x} \\ +R\left[2\sin\alpha_1-\sin\left(2\alpha_1\right)\right]C^2_{\theta_z-f_y} \\ +\cos\left(2\alpha_1\right)\cdot C^2_{u_x-f_x} + \sin\left(2\alpha_1\right)\cdot C^2_{u_x-f_y} \end{cases} \quad (9)$$

where the superscript 2 indicates the variable-thickness segment whose compliances are calculated by means of Eqs. (3) and the superscript 1 denotes the constant-thickness portion whose compliances are:

$$C^1_{\theta_z-m_z} = \frac{12R\alpha_1}{Ewt^3};\ C^1_{\theta_z-f_x} = \frac{12R^2}{Ewt^3}\cdot\left(\alpha_1-\sin\alpha_1\right);$$
$$C^1_{u_x-f_x} = \frac{12R^3}{Ewt^3}\cdot\left[3\alpha_1/2-2\sin\alpha_1+\sin\left(2\alpha_1\right)/4\right] \quad (10)$$

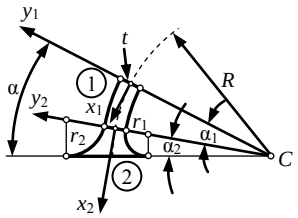

Fig. 7. Half of the circular-axis symmetric right circularly corner-filleted flexure hinge with defining geometry

Similarly to the previous flexure design, finite element analysis and experimental testing have been used to validate the analytical results corresponding to the following parameters defining a right circularly corner-filleted flexure hinge: R = 0.0889 m, $\alpha = 20^o$, $\alpha_2 = 7.122^o$, t = 0.00508 m, w = 0.00635 m, r_1 = 0.009525 m, r_2 = 0.012941 m. The material is aluminum with $E = 71 \times 10^9$ N/m^2 and μ = 0.33. The analytical, finite element analysis, and experimental results were in good agreement with a maximum error between analytical and experimental data of 6.4% corresponding to the $C_{ux\text{-}fy}$ compliance.

V. Conclusions

The paper studied the formulation of planar compliances for generic symmetric circular-axis flexure hinges. The six compliances can be expressed in terms of only three compliances defining half the symmetric flexure hinge. The general equations are utilized to derive the specific compliances for two new designs: the right circular flexure hinge and the right circularly corner-filleted flexure configuration. An experimental setup was designed to measure the compliances of the two flexure hinge prototypes and finite element simulation was also utilized. The experimental and FEA results confirmed the analytical model predictions.

References

[1] Y. Tian, B. Shirinzadeh, and D. Zhang, "A flexure-based mechanism and control technology for ultra-precision turning operation," Precision Engineering, vol. 33 (2), 2009, pp. 160-166.
[2] W. Dong, L. Sun, and Z. Du, "Stiffness research on a high-precision large-workspace parallel mechanism with compliant joints," Precision Engineering, vol. 32 (3), 2008, pp. 222-231.
[3] J. B. Hopkins and M. L. Culpeper, "Synthesis of multi-degree of freedom, parallel flexure system via freedom and constraint topology (FACT) – part II: practice," Precision Engineering, vol. 34 (2), 2010, pp. 271-278.
[4] S. Polit and J. Dong, "Development of a high-bandwith XY nanopositioning stage for high-rate micro/nanomanufacturing," IEEE/ASME Transaction of Mechatronics, vol. 16 (4), 2011, pp. 724-733.
[5] S. Bhashash and J. Jalili, "Robust adaptive control of coupled parallel piezo-flexural nanopositioning stages," IEEE/ASME Transaction of Mechatronics, vol. 14 (1), 2009, pp. 724-733.
[6] Q. Xu, "Design and development of flexure-based dual-stage nanopositioning system with minimum interference behavior," IEEE Transactions on Automation Science and Engineering, vol. 9 (3), 2012, pp.554-563.
[7] M. N. Mohd Zubir and B. Shirinzadeh, "Development of a high precision flexure-based microgripper," Precision Engineering, vol. 33 (4), 2009, pp. 362-370.
[8] D. Sun and J. K. Mills, "Manipulating rigid payloads with multiple robots using compliant grippers," IEEE/ASME Transactions on Mechatronics, vol. 7 (1), 2002, pp. 23-34.
[9] D. H. Wang, Q. Yang, and H. M. Dong, "A monolithic compliant piezoelectric-driven microgripper: design, modeling and testing," IEEE/ASME Transactions on Mechatronics, vol. 18 (1), 2013, pp. 138-147.
[10] D. Vukobratovich, R. M. Richard, J. P. Niven, and R. L. Sinclair, "Slit diaphragm flexures for optomechanics," Proceedings of SPIE: Optomechanical and Precision Instrument Design, vol. 32, 1995, pp. 278-288.
[11] S. Awtar and A. H. Slocum, "Design of flexure stages based on diaphragm flexure," Proceedings of ASPE 2005 Annual Meeting, Norfolk, VA, October 2005.
[12] B. Shusheng, Z. Shanshan, and Z. Xiaofeng, "Dimensionless design graph for three types of annulus-shaped flexure hinges," Precision Engineering, vol. 34, 2010, pp. 659-666.
[13] N. Lobontiu and M. Cullin, "In-plane elastic response of two-segment circular-axis symmetric notch flexure hinges: the right circular design, " Precision Engineering, vol. 37, 2013, pp. 542-555.
[14] N. Lobontiu, M. Cullin, M. Ali, and J. Hoffman, "Planar compliances of thin circular-axis notch flexure hinges with midpoint radial symmetry," Mechanics Based Design of Structures and Machines, vol. 41, 2013, pp. 202-221.